



HAL
open science

Power Curve Analysis Of On-ground Airborne Wind Energy Systems

Yashank Gupta, Jonathan Dumon, Ahmad Hably

► **To cite this version:**

Yashank Gupta, Jonathan Dumon, Ahmad Hably. Power Curve Analysis Of On-ground Airborne Wind Energy Systems. ICIT 2019 - IEEE International Conference on Industrial Technology, Feb 2019, Melbourne, Australia. 10.1109/ICIT.2019.8755195 . hal-01973326

HAL Id: hal-01973326

<https://hal.science/hal-01973326>

Submitted on 8 Jan 2019

HAL is a multi-disciplinary open access archive for the deposit and dissemination of scientific research documents, whether they are published or not. The documents may come from teaching and research institutions in France or abroad, or from public or private research centers.

L'archive ouverte pluridisciplinaire **HAL**, est destinée au dépôt et à la diffusion de documents scientifiques de niveau recherche, publiés ou non, émanant des établissements d'enseignement et de recherche français ou étrangers, des laboratoires publics ou privés.

Power Curve Analysis Of On-ground Airborne Wind Energy Systems

Yashank Gupta, Jonathan Dumon, Ahmad Hably
Univ. Grenoble Alpes, CNRS, Grenoble INP*,GIPSA-Lab,
F-38000 Grenoble, France.

*Institute of Engineering Univ. Grenoble Alpes
{yahsank.gupta, jonathan.dumon, ahmad.hably}@gipsa-lab.fr

Abstract—In this paper, an algorithm is proposed to control parameters of an on-ground airborne wind energy system for the operational wind speed range, considering different winch configurations and the related saturation of its components, including electrical and hydraulic devices. Coupled with a static model, this leads to a tool that can easily calculate expected power curves for on-ground airborne wind energy system as a function of design parameters. The paper also presents the numerical examples of the power curve for a Magnus-based system and draws a comparison with the power curves of horizontal axis wind turbines.

Index Terms—Airborne wind energy system, On-ground system, pumping system, Power curve, Ground station design, Magnus effect, Static modeling, High-level control, Hydraulic stage

I. INTRODUCTION

Airborne wind energy systems (AWE) aims at proposing a complementary solution to the conventional wind turbines. AWE systems harness the energy of high altitude winds by using an airborne platform connected to the ground by tethers or conducting cables. AWE systems have attracted a lot of interest in the last few decades (see [1] for a survey on soft kites and [2] for AWE systems in general).

Depending on the location of energy production, AWE systems can be divided into two main classes: On-ground production and On-board production AWE systems. On-ground production systems consist of a ground-based generator connected to an airborne platform by tethers. Whereas in the on-board production systems, the turbine is mounted on the airborne platform. Currently, in the research community, there are many innovative designs regarding the airborne platform. The choice of the platform depends on the lifting capabilities of the aerodynamic surface. Classically, kites and unmanned aerial vehicles (UAV) have been used as the airborne platform. But with an increased interest in AWE usage of many innovative concepts are being explored such as Magnus cylinders, rotary kites, balloons etc.

Power curves serve as a tool to analyze the economic feasibility of any type of wind turbine. In literature, there are many studies discussing the power curves of conventional wind turbines. Over the years, the power curves have been validated and improved by incorporating the on-field data from the installed wind turbines. To evaluate the economic viability of airborne wind energy systems, and to draw valid comparisons with the conventional turbines, there is a need to develop accurate power curves for AWE systems. Currently, there are very few working prototypes of AWE systems and none of them is a fully functioning commercial unit. Thus, the power curves for AWE systems are still an open topic of discussion in the research community. In [3] a study is presented discussing the family of power curves for different altitudes derived from a model presented in [4]. The study also compares the

power curves with the dynamic simulations of the Enerkite AWE prototype EK30 and it concludes that the significant confidence can be placed on the approach presented in the work for estimating the power curves for AWE systems. In [5] a simplified model is analyzed to estimate the maximum feasible drag power for an on-board production system. In [6] an optimal control problem is discussed which is then used to obtain power curves for a rotary kite AWE system. In the authors' previous work [7], a strategy to control the power production of a Magnus-based AWE system is proposed. In [8], the authors propose a 6-DOF mathematical model for the Magnus based AWE system validated by simulation, controlling the system in crosswind trajectories. A static model of the full cycle is presented and compared to the dynamic simulation. In this present study, based on a static model proposed and validated in [8] and a structural analysis of ground station structure, including electrical and hydraulic solutions, a generic static model of on-ground AWES is proposed. A high-level algorithm is the developed to maximize the net output power of the system, taking into consideration the necessary saturation of the system. This fast model can then be used to calculate power curves of on-ground AWES in function of different design parameters. As authors are working specifically on Magnus-based on-ground AWE systems, numerical application for these type of systems is done to draw comparisons with conventional horizontal axis wind turbines. The power curves calculated in this paper give a valuable insight into the potential of AWE systems and expose some advantages over conventional wind turbines.

The paper is organized as follows. Section II focuses on the modeling of the different parts of the system. In section III, the control and the optimization of the output power are presented. A numerical application follows in section IV. The paper ends with some conclusions in section V.

II. MODELLING

A. Model of Wind Profile

In this paper, wind profile power law is considered to describe the evolution of horizontal mean wind speed with altitude. This theoretical model is discussed in detail in literature [9] and provides a good approximation of the wind speed for the altitudes between 100 to 2000 m. According to this model, the wind speed V_w at any altitude z can be given by:

$$V_w(z) = V_w(z_0) \left(\frac{z}{z_0}\right)^\alpha \quad (1)$$

Where, z_0 represents the operating altitude, $V_w(z_0)$ is the known wind speed at altitude z_0 , and α is an empirically derived coefficient that characterizes the surface. It depends on the stability of the atmosphere and is generally assumed to be equal to 0.143. To take into account the constant variation of the wind speed and to calculate the mean wind speed at a particular site throughout the year, the well know Weibull distribution is used in this paper. The distribution basically tells at a

particular site how often the wind blows and how strong it is. Thus, it is a good way to describe the wind speed variations and it is given by:

$$f(v) = \frac{k}{a} \left(\frac{v}{A} \right)^{k-1} e^{-\left(\frac{v}{A}\right)^k} \quad (2)$$

Where, $f(v)$ is a probability to have v wind speed over the year, A is the Weibull scale parameter expressed in m/s and is proportional to mean wind speed, and k is the Weibull form parameter describing the shape of the Weibull distribution with its value between 1 and 3. Smaller values of k show very variable winds while larger values show constant winds. Finally, v is the wind speed series whose probability distribution is calculated.

B. Model of a Horizontal axis wind turbine (HAWT)

For conventional wind turbines, the power produced depends on the kinetic energy of the air and C_p the power coefficient of the turbine which is smaller than its theoretical Betz limit 16/27:

$$P_{HAWT} = \frac{1}{2} \rho C_p A_{swept} V_w^3 \quad (3)$$

Where, A_{swept} is the total surface swept by the blades. Power produced, P_{HAWT} , is generally divided into four phases characterized by the design constraints of the system. The first phase is from zero wind speed to cut-in wind speed V_{ci} , where a conventional turbine does not produce any energy. The second phase is from V_{ci} to the nominal wind speed V_{nom} , where the maximum wind power extraction occurs by maximizing C_p coefficient. The third phase is from V_{nom} to the cut-off wind speed V_{co} , and during this phase power is curtailed to nominal power P_{nom} by reducing C_p coefficient. Finally, for any wind speed beyond V_{co} , the wind turbine is switched-off to avoid its mechanical and electrical degradation. Therefore, the power curves of a HAWT can be produced by the following set of equations:

$$P_{HAWT} = \begin{cases} \frac{1}{2} \rho C_{pmax} A_{swept} V_w^3 & \text{if } V_{ci} < V_w \leq V_{nom} \\ P_{nom} & \text{if } V_{nom} < V_w < V_{co} \\ 0 & \text{if } V_w \geq V_{co} \text{ or } V_w \leq V_{ci} \end{cases} \quad (4)$$

C. Static Model of Ground-based Airborne Wind Energy System

The production cycle for any on-ground AWE system is divided into two phases, namely, the production phase and the recovery phase. The production phase is characterized by reeling out the tether from the on-ground station while following a crosswind trajectory in the air. As a result, a traction force is produced in the tether attached to the airborne platform which is then used to generate electricity. In the recovery phase, the airborne platform is pulled back to the on-ground station. Thus, a part of the power produced during the production phase is consumed during the recovery phase. In order to minimize the energy consumption during this phase, the traction force has to be minimized.

Aerodynamic lift and drag forces acting on any classical airborne platform (such as kite, rigid wing, UAV or Magnus cylinder etc.) can be expressed as:

$$L = \frac{1}{2} \rho S V_a^2 C_L, \quad D = \frac{1}{2} \rho S V_a^2 C_{Deq} \quad (5)$$

Where, ρ is the air density, V_a is the apparent wind velocity, S is the projected surface of the airborne platform, C_L is its aerodynamic lift coefficient, and C_{Deq} is equivalent aerodynamic drag coefficient of the system including the drag due to the tether and any other structural components of the airborne platform. Note that C_{Deq} has to be expressed in function of tether length to consider additional drag effect for each additional tether length.

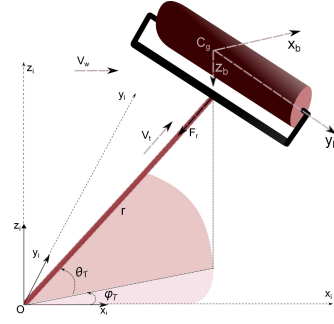


Fig. 1. Magnus-based AWE system.

The component of the wind in the direction parallel to the tether, as experienced by the platform, can be expressed as:

$$V_t = V_w \cos(\theta_T) \cos(\phi_T) \quad (6)$$

Where, θ_T and ϕ_T represents the elevation and the azimuthal angle of the tether with respect to the inertial frame. Figure 1 presents a 3D model of a Magnus-based AWE system described using two frames of references. Inertial frame, (x_i, y_i, z_i) , centered at the ground station O , and a body frame, (x_b, y_b, z_b) , centered at the center of gravity C_g of the system. The tether length is presented by variable r which can be expressed as:

$$r = \sqrt{x^2 + y^2 + z^2} \quad (7)$$

Where, (x, y, z) are the coordinates of C_g in the inertial frame. In the static analysis of [8], assuming straight taut tether, the traction force F_r developed in the tether is directly proportional to the resultant aerodynamic force acting on the Magnus cylinder. Thus, the total mechanical energy available at the winch of the on-ground station is given by $P = F_r \dot{r}$. Where, \dot{r} represents the reel-in or reel-out speed of the tether.

1) *Production phase*: The power produced by any AWE during a production phase is given by:

$$P_{prod} = F_r \dot{r}_{prod} \quad (8)$$

Where, \dot{r}_{prod} refers to the reeling-out speed of the tether from the winch. F_r refers to the traction force developed in the tether due to the resultant aerodynamic forces. Considering the reel-out speed \dot{r}_{prod} , the power produced during the production phase is given by:

$$P_{prod} = \frac{1}{2} \rho S (V_t - \dot{r}_{prod})^2 C_L \left(\frac{C_L}{C_{Deq}} \right)^2 \dot{r}_{prod} \quad (9)$$

Here it is important to note that this static power equation first derived in [4] and further refined in [10] is obtained by using equilibrium motion theory for crosswind maneuver. It does not take into account the contribution of the centrifugal force acting on the airborne platform. In addition, it is assumed that the wind is parallel to the tether and the AWE system is assumed in the static state. Thus, a detailed analysis considering all the effects may yield a better expression for power produced by an AWE system. For the production phase, the maximum possible theoretical mechanical power that can be produced for a given set of lift and drag coefficients C_L and C_{Deq} is studied in [4]. In [10] it is proved that for maximum power the reel-out speed of the tether, \dot{r}_{prod} , should be equivalent to $\frac{V_w}{3}$ while the AWE system follows a crosswind trajectory such as circles or eight-like figures perpendicular to the wind direction. Thus, following this assumption the maximum theoretical mechanical power produced can be expressed by:

$$P_{prod} = \frac{1}{2} \rho \frac{4}{27} S V_t^3 C_L \left(\frac{C_L}{C_{Deq}} \right)^2 \quad (10)$$

However, this maximizes only the production phase and not the total power produced during the full cycle, as discussed later in section III.

2) *Recovery phase*: In the recovery phase, the airborne platform is returned to its initial position .i.e. the tether length is brought to its initial value. In this maneuver, a portion of the energy produced during the production phase is consumed. The power consumed can be calculated as the product of the winding speed of the tether \dot{r}_{rec} and the resulting drag force of the system through the tether F_{drag} :

$$P_{rec} = F_{drag}\dot{r}_{rec} \quad (11)$$

$$P_{rec} = \frac{1}{2}\rho S(V_t + \dot{r}_{rec})^2 C_{Drec}\dot{r}_{rec} \quad (12)$$

Where, C_{Drec} is the resulting drag coefficient during the recovery phase. Note that in this formulation, as \dot{r}_{rec} is negative and F_{drag} is positive, so P_{rec} is negative.

There are several operational strategies proposed in the literature to minimize the energy consumption during the recovery phase for different types of AWE system. For instance, in case of soft kites based AWE systems to minimize the energy consumption, generally, the kite is flown to the zenith to the limits of the wind window before commencing the reel-in of the tether.

In case of a Magnus-based system, in order to minimize the power consumption, the rotational speed of the Magnus cylinder, ω_{cyl} is simply set to zero, leading to lift coefficient C_L zero. Thus, minimizing the resulting drag. In [8], this type of maneuvers is performed in dynamic simulations.

Depending on the choice of airborne platform and recovery strategy, P_{rec} might have to be modified to incorporate all the effects and variables arising due to maneuvers performed for the recovery phase. This model is adapted to a platform that can be configured with no or very low lift coefficient during the recovery phase. It can be replaced by another static model of the recovery phase, such as the one proposed in [3] that includes a given set of lift and drag coefficients and a necessary additional transition time.

D. Ground-based Airborne Wind Energy System design constraints

The ground station is a reversible winch that produces energy when the airborne platform is pulling the tether, and during the recovery phase, it produces a retraction force to reel-in the tether to the drum. Actuators to be used will have saturations that are chosen to represent the following parameters:

- The nominal rotational speed ω_{nom}
- The nominal torque Γ_{nom}
- The efficiency η which depends on the actuator's rotational speed ω and torque Γ

The saturation on traction force, F_{max} , and reel-out and reel-in speed, \dot{r}_{max} , are dependant on the design of the ground station. They have to be considered in the control algorithm. Note that the system must be designed in such a way that $F_{max} = R_d\Gamma_{nom}$, and $\dot{r}_{max} = R_d\omega_{nom}$, where R_d is the radius of winch's drum. On the other hand, the tether and the airborne platform must be able to withstand the maximum traction force F_{max} . In this work, two configurations for the ground station architecture are considered. In the first one, an electrical motor-generator is used for both the phases .i.e. production and recovery phase. In the second configuration, each phase uses a separate device .i.e. an electrical generator with a gearbox optimized for production phase and an electrical motor with a gearbox optimized for the recovery phase. In this case, saturation for the each phases has to be differentiated as $F_{prod,max}$, $\dot{r}_{prod,max}$, $F_{rec,max}$ and $\dot{r}_{rec,max}$. Note that the same differentiation has to be done if a single motor is coupled with two different gearboxes.

The winch-generator system then can be directly connected either to the grid or to a local storage device which can be used to provide the power required during the recovery phase and the mean power to the

grid. The system is then able to provide a constant power during all the cycle. In this case, no power is taken from the grid, thus, ensuring a unidirectional connection to the grid. Figure 2 presents the configuration with two separate electrical actuators for the two phases and a local storage device.

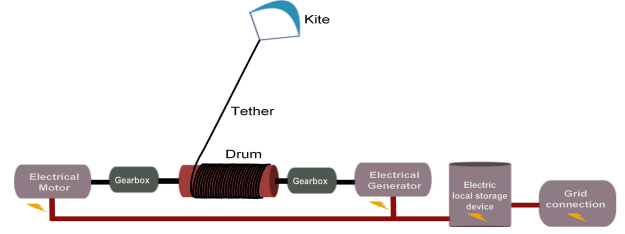


Fig. 2. Ground station using two separate electrical actuators and a storage device

In an another approach, proposed in [11], use of a hydraulic stage between the drum and the grid connection is considered. Figure 3 shows the configuration with a variable speed hydraulic motor/pump coupled with a hydraulic accumulator and a fixed speed motor which produces electricity which is then fed directly to the grid. Thanks to the emerging high efficiency digital hydraulic devices, the authors expect substantial cost reductions in the cost of both actuators and storage devices. From a control point of view, as the same actuator is used for both the phases, this leads to $F_{prod,max} = F_{rec,max}$ and $\dot{r}_{prod,max} = \dot{r}_{rec,max}$. As

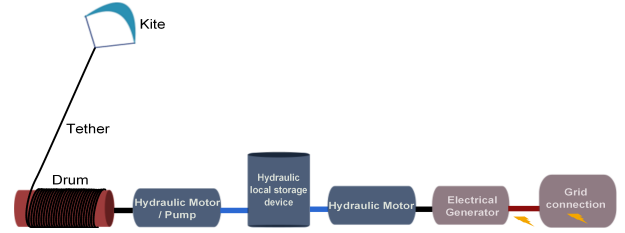


Fig. 3. Ground Station using hydraulic stage

electrical as well as hydraulic actuators has a yield that can vary with operating speed and torque, we can define for all these configurations common parameters η_p , yield of the generator (or pump) used during production phase, η_r yield of the motor used during recovery phase, η_s yield of the storage device and η_g yield of the grid connection. For hydraulic case, yield of grid connection includes hydraulic motor, electrical generator and grid connection itself.

1) *Full production cycle*: A given power cycle is thus defined by one complete production and recovery phase. The transitional phase between the production and the recovery phase is neglected in this formulation. The time for each phase can then be expressed as:

$$t_1 = \frac{r_{max} - r_{min}}{\dot{r}_{prod}} = \frac{\Delta r}{\dot{r}_{prod}} \quad (13)$$

$$t_2 = \frac{r_{max} - r_{min}}{\dot{r}_{rec}} = \frac{\Delta r}{\dot{r}_{rec}} \quad (14)$$

Where, t_1 and t_2 represent the duration of the production and recovery phase respectively. Thus, the total time, t taken for one complete production cycle is:

$$t = t_1 + t_2 \quad (15)$$

The net output power provided to the grid P_{cycle} can then be calculated by the sum of power produced affected by its yield, power consumed also affected by the inverse of its yield and the yield of storage device, and additional power loss in the storage device P_{loss} . This is due to the

storage of the necessary energy that has to be provided to the grid during recovery phase. Its expression is given in equation (16).

$$P_{loss} = \frac{P_{cycle} t_2 (\eta_s^{-1} - 1)}{t_1 + t_2} \quad (16)$$

Hence, the mean power produced during one full production cycle can be computed as:

$$P_{cycle} = \eta_g \frac{\eta_p P_{prod} t_1 + \eta_r^{-1} \eta_s^{-1} P_{rec} t_2 - P_{cycle} t_2 (\eta_s^{-1} - 1)}{t_1 + t_2} \quad (17)$$

Where, replacing the values of t_1 and t_2 from equations (13) and (14) into (17), the power produced in one complete cycle can be expressed as:

$$P_{cycle} = \eta_g \frac{\eta_p P_{prod} \dot{r}_{rec} + \eta_r^{-1} \eta_s^{-1} P_{rec} \dot{r}_{prod}}{\dot{r}_{rec} + \eta_s^{-1} \dot{r}_{prod}} \quad (18)$$

Note that from equation (18) it can be observed that in order to obtain maximum power from one complete cycle, there is a trade-off between \dot{r}_{rec} and \dot{r}_{prod} . Hence, the augmentation of \dot{r}_{rec} not only increases the contribution of the production phase but also increases the value of the power consumed P_{rec} as given by equation (12). Similarly, increasing \dot{r}_{prod} not only increases the power produced as expressed by equation (9) but also the power consumed.

III. CONTROL AND OPTIMIZATION OF OUTPUT POWER

As explained in the section II, for a ground-based AWE system, the net power produced in one cycle depends on physical parameters, design parameters, and controllable parameters. All controllable parameters of P_{prod} described in equation (9) must maximize P_{prod} , except reel-out speed \dot{r}_{prod} which also influences the whole cycle through P_{rec} . This leads to maximization of $\cos(\theta_T) \cos(\phi_T)$ and $C_L \left(\frac{C_L}{C_{Deq}} \right)^2$. Similarly, all controllable parameters of P_{rec} described in equation (12) has to minimize it, except reel-in speed \dot{r}_{rec} which also influences the whole cycle through P_{prod} . In this phase, $\cos(\theta_T) \cos(\phi_T)$ and C_{Drec} has to be minimized. Thus, to obtain the maximum mean power, it is necessary to obtain optimal values of \dot{r}_{prod} and \dot{r}_{rec} . In this section, a high level algorithm is described, using all control parameters available for on-ground AWE systems in presence of saturation. An optimization technique is discussed for three separate situations which characterizes different typical constraints due to on-ground winch and airborne platform design, namely:

- Optimize both \dot{r}_{rec} and \dot{r}_{prod}
- Optimize \dot{r}_{prod} when \dot{r}_{rec} is set
- Optimize \dot{r}_{rec} when \dot{r}_{prod} is set

A. No saturation on actuators: Optimization of reel-in and reel-out speeds

To maximize the net power production during one complete cycle, \dot{r}_{prod} and \dot{r}_{rec} has to be optimized simultaneously. In the considered optimization procedure, P_{cycle} is derived with respect to each \dot{r}_{rec} and \dot{r}_{prod} while considering the other variables as constant.

$$\frac{\partial P_{cycle}}{\partial \dot{r}_{rec}} = f(V_w, \dot{r}_{rec}, \dot{r}_{prod}, M) \quad (19)$$

while considering \dot{r}_{prod} , V_w and the vector of parameters M as constant. Vector M is given by:

$$M = [C_L, C_{Deq}, C_{Drec}, \phi_T, \theta_T, \eta_p, \eta_r, \eta_s, \eta_g, \rho, S] \quad (20)$$

Similarly,

$$\frac{\partial P_{cycle}}{\partial \dot{r}_{prod}} = f(V_w, \dot{r}_{rec}, \dot{r}_{prod}, M) \quad (21)$$

while considering this time that \dot{r}_{rec} as constant. The first order partial derivative results in a polynomial function, and solving the system of equation gives the optimal values of \dot{r}_{rec} and \dot{r}_{prod} :

$$\begin{cases} \dot{r}_{rec_{opt}} = f_s(V_w, \dot{r}_{prod}, M) \\ \dot{r}_{prod_{opt}} = g_s(V_w, \dot{r}_{rec}, M) \end{cases} \quad (22)$$

B. Optimization of reel-in speed when reel-out speed is set

As presented before, the power produced by an AWE system in production phase is given by:

$$P_{prod} = F_r \dot{r}_{prod} \quad (23)$$

Due to design and structural constraints, there exists an upper limit for traction force F_r denoted by F_{max} . This limit can be attributed to tether, winch and/or kite structural limitations. When this limit is reached during the production phase, and if $\cos(\theta_T) \cos(\phi_T)$ and $C_L \left(\frac{C_L}{C_{Deq}} \right)^2$ are set at their maximum value, then \dot{r}_{prod} has to be set such that $F_r = F_{max}$, and it can be calculated using equation (9):

$$\dot{r}_{prod} = V_t - \sqrt{\frac{F_{max}}{\frac{1}{2} \rho S C_L \left(\frac{C_L}{C_{Deq}} \right)^2}} \quad (24)$$

In this case, if \dot{r}_{prod} reaches $\dot{r}_{prod_{max}}$ then it can be saturated, but F_r has to be maintained equal to F_{max} . This can be done by reducing other parameters such as $\cos(\theta_T) \cos(\phi_T)$ or $C_L \left(\frac{C_L}{C_{Deq}} \right)^2$. Thus, in this case in order to maximize P_{cycle} the reel-in speed has to be optimized for $F_r = F_{max}$ and \dot{r}_{prod} given by equation (24). The optimal reel-in speed $\dot{r}_{rec_{opt1}}$ can be found by:

$$\frac{\partial P_{cycle}}{\partial \dot{r}_{rec}} = f_1(V_w, \dot{r}_{prod}, r_{rec}, F_r, M) \quad (25)$$

where, P_{cycle} is calculated from equation (18) with a saturation on traction force and is calculated as:

$$P_{cycle} = \eta_g \frac{\eta_p F_{max} \dot{r}_{prod} \dot{r}_{rec} + \eta_r^{-1} \eta_s^{-1} P_{rec} \dot{r}_{prod}}{\dot{r}_{rec} + \eta_s^{-1} \dot{r}_{prod}} \quad (26)$$

and, the optimal reel-in speed $\dot{r}_{rec_{opt1}}$ is given by:

$$\dot{r}_{rec_{opt1}} = f_{s1}(V_w, \dot{r}_{prod}, F_r, M) \quad (27)$$

Similarly, if \dot{r}_{prod} reaches $\dot{r}_{prod_{max}}$ before the saturation of traction force F_r then $\dot{r}_{rec_{opt1}}$ is calculated from equation (27), using $\dot{r}_{prod} = \dot{r}_{prod_{max}}$ and F_r are calculated from eqs. (8) and (9).

C. Optimization of reel-out speed when reel-in speed is set

In some situations, reel-in speed is required to be saturated to $\dot{r}_{rec_{max}}$, before other variables like traction force or reel-out speed reach their upper limit. As optimal reel-in speed can be several times higher than the reel-out speed, especially in the case when the ground station uses the same actuator for production and recovery phases .i.e. without a two-stage gearbox. In such situations, the reel-in speed can reach its upper limit before the traction force. Thus, in this case the optimal $\dot{r}_{prod_{opt2}}$ has to be calculated using equation (22) and $\dot{r}_{rec_{max}}$:

$$\dot{r}_{prod_{opt2}} = g_{s2}(V_w, \dot{r}_{rec_{max}}, M) \quad (28)$$

Here it is important to note that in this case it is mandatory to check other variables for saturation. Thus, if $\dot{r}_{prod_{opt}} > \dot{r}_{prod_{max}}$ then $\dot{r}_{prod_{opt}}$ has to be set to $\dot{r}_{prod_{max}}$. On the other hand, by using equation (9) if the traction force is found to be greater than its maximum i.e. $F_r > F_{max}$. Then \dot{r}_{prod} has to be calculated by using equation (24).

D. Control by using altitude

Control of working altitude can be done by controlling r_{min} and r_{max} parameters i.e. minimum and maximum tether length. This can be done in order to find an altitude that maximizes power produced or to curtail production by lowering wind speed when it is necessary. Thus, there is a maximal effective wind speed $V_{t,max}$ beyond which P_{cycle} starts to decrease despite of the augmentation of wind speed. This is due to the fact that at $V_{t,max}$, due to all the design constraints, the production phase saturates while the power required for the recovery phase continues to grow with the increase in wind speed. Seeking an altitude where the wind is lower is useful when the wind is greater than the optimal wind speed of the system.

E. Control of elevation angle θ_T or azimuthal angle ϕ_T

To curtail output power or reduce effective wind speed, the trajectory of the airborne platform can be controlled, in order to modify elevation angle θ_T or azimuthal angle ϕ_T . This gives an additional control variable in order to operate on-ground AWES.

F. Summary Of The High-Level control algorithm

A high-level control strategy to maximize net power production P_{cycle} in presence of multiple actuator saturation for all operating wind speed range presented in this section can be summed as the following. Reel-in and reel-out speed has to be optimized, taking into account system saturations. With both reel-in and reel-out are saturated, control of altitude z , elevation angle θ_T , and/or azimuthal angle ϕ_T can be used to maintain output power to its nominal value.

IV. NUMERICAL APPLICATION

In this section, different set of parameters of Magnus-based on-ground airborne wind energy system (MGAWES) are considered. Power curves, annual production, and capacity factor are compared with those of similar size horizontal axis wind turbine (HAWT).

A. HAWT parameters

VESTAS V150 – 4.2MWTM, designed for IEC IIIB wind class, is chosen as HAWT system to be compared with on-ground AWES. Corresponding parameters presented in table are taken from [12] or deduced from power curve data set in [13].

	Variable	Value
Nominal Power [MW]	P_{nom}	4.2
Cut-in wind speed [m/s]	V_{ci}	3
Cut-out wind speed [m/s]	V_{co}	22.5
Rotor diameter [m]	D_{HAWT}	150
Tower height [m]	h	160
Power coefficient	C_p	0.45

TABLE I
PARAMETERS OF HAWT VESTAS V150 – 4.2MWTM.

B. Wind parameters

Wind is considered at an altitude at the tower height i.e. 160m with mean annual wind speed 7.5m/s. For annual production, Weibull distribution is used with parameters $A = 8, 47m/s$ and $k = 2$, which leads to class IIIB.

C. 90m span MGAWES parameters

The parameters considered are listed in table II. Aerodynamical parameters are taken from [14], and for the sake of comparison, some other parameters are designed to get the same power curve as for the considered HAWT for wind speeds varying from V_{ci} to V_{nom} . Also, for the same reason same cut-in and cut-out wind speeds are used.

Two types of ground stations as described in section II-D are considered. One with two separate electrical actuators, and other with hydraulic stage with their apifications also listed in table II.

Kite parameters	Variable	Value
Span [m]	L	90
Radius [m]	R	9
Magnus Surface [m ²]	S	1620
Maximum $C_L \left(\frac{C_L}{C_{Deq}} \right)^2$ for $X = 3.6$	$C_L \left(\frac{C_L}{C_{Deq}} \right)^2$	69.44
Minimum drag coefficient	C_{Drec}	0.5
Minimum elevation angle [deg]	θ_T	25
Cut-in wind speed [m/s]	V_{ci}	3
Cut-out wind speed [m/s]	V_{co}	22.5
Maximal traction force [kN]	F_{max}	2405
Maximal strength [N/m ²]	σ	1485
Working altitude [m]	z	160
Aspect ratio	AR	5
Reynolds number for $V_a = 10m/s$	Re	10.9e6

Case 1: Ground station with 2 electrical actuators

Electric generator nominal power [MW]	$P_{prod,max}$	10
Nominal Power for grid connection [MW]	P_{grid}	5.91
Electric motor nominal power [MW]	$P_{rec,max}$	5.56
Yield of generator	η_p	0.92
Yield of motor	η_r	0.88
Yield of storage device	η_s	1
Yield of grid connection	η_g	0.98
Maximal reel-in speed [m/s]	$\dot{r}_{rec,max}$	14.7
Maximal reel-out speed [m/s]	$\dot{r}_{prod,max}$	4.16

Case 2 : Ground station with hydraulic stage

Electric generator nominal power [MW]	P_{grid}	10.9
Hydraulic motor/pump nom. power [MW]	P_{max}	40
Yield of motor/Pump for production	η_p	0.92
Yield of motor/Pump for recovery	η_r	0.88
Yield of storage device	η_s	1
Yield of grid connection	η_g	0.98
Maximal reel-in and reel-out speed [m/s]	\dot{r}_{max}	16.65

TABLE II
PARAMETERS OF THE 90M SPAN MGAWES.

D. Results

Power curves of HAWT V150 both with theoretical model and dataset are plotted in figure (4). Power curves derived using P_{cycle} for a 90m span MGAWES for case 1 and case 2 ground station configuration are also plotted in figure (4). As case 1 represents a more relevant example of different configurations of saturation expressed in section III, thus, for this case P_{prod} and P_{rec} are also plotted in figure (4). To describe the 4 different phases of the power curve, denoted by I to IV, reel-in and reel-out speed, traction forces and elevation angle are shown on figure (5).

As it can be observed from figure (4) phase II of HAWT and MGAWES are very similar. This is because in this phase, just like HAWT, MGAWES is a function of V_w^3 , and an optimal amount of kinematic energy is extracted from the wind. During phase III, the traction force is saturated, but P_{prod} continues to increase as reel-out speed increases with an increasing wind speed. In phase IV, once the maximum P_{prod} is reached then only P_{rec} increases as with an increase in the wind speed the drag also increase. Thus, more and more power is required to recover the airborne platform. This leads to a reduction in the net power output P_{cycle} as represented by dotted line in figures (4) and (5). Finally, solid

lines in phase IV shows the use of elevation angle θ_T control, to maintain the effective wind V_t at its maximal value in order to maintain output power at its maximum. In table II, case 2 represents the case when there are no set limitations on the winch actuators. This set of parameters are chosen to illustrate hydraulic configuration because for both the phases actuator is same. So, the winch actuators have to at least produce the high force F_{max} and high speed $r_{rec,max}$ in the same time. This extends the phase III to maximum cut-out value V_{co} . The maximum output power is then produced at this maximum wind speed, and has to be used to size the grid connection P_{grid} . Note that the same power curve can be produced with a single 40MW electric motor/generator coupled with a single gearbox. Using these theoretical power curves and wind distribution described in subsection IV-B, the theoretically expected energy produced during one year can be computed for HAWT V150 and different ground-station configurations for the same 90m span Magnus effect kite. In particular, it is interesting to note that just for the sake of comparison, using figure (4), the use of a generator and a motor that saturates at the same wind speed as HAWT (i.e. $P_{prod,max} = 6.7MW$ and $P_{rec,max} = 4MW$) will lead to a similar power curve and similar annual production. This configuration is considered as case 0. Table III summarizes the different systems considered and associated size of actuators. It also gives the corresponding theoretical annual production and capacity factor, computed by annual production divided by $8760P_{grid}$.

System	P_{Grid} [MW]	Generator [MW]	Motor [MW]	Prod. [GWh/yr]	Capacity factor
Vestas V150	4.2	4.2	-	18.2	0.49
AWES Case 0	4.2	6.7	4	18.2	0.49
AWES Case 1	5.9	10	5.56	21.9	0.42
AWES Case 2	10.9	40	-	24.8	0.26

TABLE III

CONSIDERED ACTUATORS CONFIGURATIONS AND CORRESPONDING THEORETICAL ANNUAL PRODUCTION AND CAPACITY FACTOR

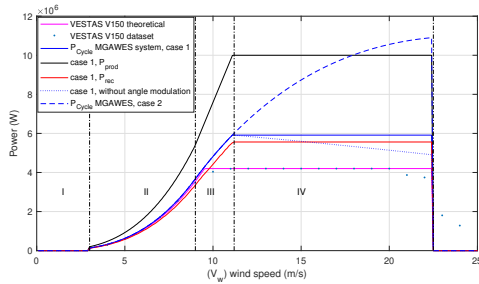


Fig. 4. Power curves: Power production comparison between HAWT Vestas V150 and case 1 and case 2 of MW-size MGAWES. P_{cycle} is decomposed into production and recovery contributions for case 1. Dotted line denotes P_{cycle} when control of elevation angle is not used

V. CONCLUSION

In this work, a static model is proposed as a simple tool that can be used to predict the performance of the on-ground AWES in relation to the main design parameters. The proposed algorithm gives a strategy to maximize the energy produced by this kind of system for different configurations of actuator saturation under the static assumption. By coupling the static model with the high-level algorithm, a way to calculate power curves is presented. This approach is used to study the effects of design parameters on performances and can be used directly to control a system in real-time. The resulting power curves consist

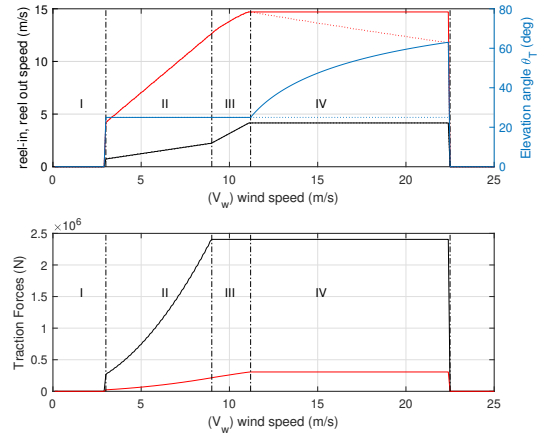


Fig. 5. High level control variables of case 1, 90m span MGAWES. Top: reel-out speed during production phase (black) and reel-in speed during recovery phase (red) in function of wind speed. Dotted line represents variables when control of elevation angle is not used. Down: Traction force during production (black) and recovery (red) phases.

of different phases, each phase corresponding to the different control variables, and illustrates the high flexibility of on-ground airborne wind energy system.

The strategy presented can be used to evaluate other types of AWE systems and draw some valid comparisons with conventional wind turbines.

REFERENCES

- [1] M. Ahmed, A. Hably, and S. Bacha, "High altitude wind power systems: A survey on flexible power kites," in *2012 XXth International Conference on Electrical Machines*, Sept 2012, pp. 2085–2091.
- [2] A. Cherubini, A. Papini, R. Verthey, and M. Fontana, "Airborne wind energy systems: A review of the technologies," *Renewable and Sustainable Energy Reviews*, vol. 51, pp. 1461–1476, 2015.
- [3] M. Ranneberg, D. Woffle, A. Bormann, P. Rohde, F. Breipohl, and I. Bastigkeit, "Fast power curve and yield estimation of pumping airborne wind energy systems," vol. AWEC, 2017.
- [4] M. Loyd, "Crosswind kite power," *J. ENERGY*, vol. 4(3), 1980.
- [5] F. Bauer, R. M. Kennel, C. M. Hackl, F. Campagnolo, M. Patt, and R. Schmehl, "Drag power kite with very high lift coefficient," *Renewable Energy*, vol. 118, pp. 290 – 305, 2018.
- [6] J. De Schutter, R. Leuthold, and M. Diehl, "Optimal control of a rigid-wing rotary kite system for airborne wind energy," 03 2018.
- [7] A. Hably, J. Dumon, and G. Smith, "Control of an airborne wind energy system with a Magnus effect," in *The 2016 American Control Conference*, Boston, United States, Jul. 2016. [Online]. Available: <https://hal.archives-ouvertes.fr/hal-01272253>
- [8] Y. Gupta, J. Dumon, and A. Hably, "Modeling and control of a magnus effect-based airborne wind energy system in crosswind maneuvers," *IFAC-PapersOnLine*, vol. 50, no. 1, pp. 13 878–13 885, 2017.
- [9] C. L. Archer, "An introduction to meteorology for airborne wind energy," in *Airborne Wind Energy*, 2013, pp. 81–94.
- [10] I. Argatov, P. Rautakorpi, and R. Silvennoinen, "Estimation of the mechanical energy output of the kite wind generator," *Renewable Energy*, vol. 34, pp. 1525–1532, 2009.
- [11] M. A. Tattersfield, J. F. Atwater, and C. P. Houle, "Method and system for harnessing wind energy using a tethered airfoil," Jun. 2 2015, uS Patent 9,046,072.
- [12] VESTAS, "<https://www.vestas.com/en/products/turbines>," 2018.
- [13] windparka, "<http://www.windparka15lingewaard.nl>," 2018.
- [14] M. Milutinović, M. Corić, and J. Deur, "Operating cycle optimization for a magnus effect-based airborne wind energy system," *Energy Conversion and Management*, vol. 90, pp. 154–165, Jan 2015.